Vibration analysis of beam structures with localized nonlinearities by a wave approach

B. Chouvion

Vibration analysis of beam structures with localized nonlinearities by a wave approach

B. Chouvion

Ecole Centrale de Lyon, LTDS, CNRS UMR 5513, 69 130, Ecully, France

Keywords:
Nonlinear dynamics
Waveguide structures
Wave scattering
Nonlinear waves
Localized nonlinearities
Harmonic balance

A B S T R A C T

This paper presents a general wave propagation approach for the vibration analysis of structures consisting of beam elements with localized nonlinearities. The scattering of a wave at a nonlinear discontinuity creates multi-harmonic waves. This forms the basis of the model formulation in which the displacement in each element composing the structure is defined as a sum of waves associated with the fundamental frequency and its harmonics. The coupling between separate elements is expressed using transmission coefficients function of the harmonic number and includes propagating and decaying near field waves whose amplitudes are the unknowns of the problem. With the use of harmonic balance, a characteristic algebraic equation of motion is derived. The general systematic methodology is demonstrated and detailed on beam-like systems with nonlinear boundaries for validation against a conventional finite element analysis. To illustrate the effectiveness of the approach on a more practical case, the method is also applied to a simplified model of a turbomachinery blade with underplatform friction dampers. The predictions of stick-slip effect and global nonlinear damping behavior made using the proposed approach are shown to be in excellent agreement with the results of numerical time integration with the advantage of reduced computational costs.

1. Introduction

Complex three-dimensional (3D) structural designs are often initially modeled for pre-dimensioning as simple assemblages of waveguide components such as beams, bars or rings, before going through a final validation generally performed with a full and expensive 3D finite element (FE) model. Using a simple model in the first step of the design process is even more relevant in nonlinear applications where the numerical cost can become prohibitive. Recent uses of beam-like models with localized nonlinearities appear in various fields. This include for instance a schematic representation of bladed disk-casing interaction [1,2] or friction in blade shrouding [3] in aircraft or helicopter engine applications; and defect detection in structural health monitoring [4] via the nonlinear interaction of elastic waves. In addition, many engineering structures can also be directly modeled as beam-like network. In recent applications dealing with nonlinear vibrations, one could cite for instance a piezoelectric cantilever beam with a moving magnet at its free end [5] or impacting on a mechanical stop [6,7] in MEMS energy harvesting application; micro-vibro-impacts and frictional slips of Euler-Bernoulli beams [8]; and passive control of vibrations of beams using the concept of nonlinear energy sink [9]. In all of these different applications, the key component is a beam-like structure whose design and optimization could be aided greatly by the availability of efficient techniques to rapidly determine the effects of variations in geometry and dimensions on vibration characteristics, in both linear and nonlinear regimes.

E-mail address: benjamin.chouvion@ec-lyon.fr.

The nonlinear vibrational response of simple structures such as uncoupled beams with added stiffnesses and masses is generally approximated using Rayleigh-Ritz or modal approaches solved by different techniques depending on the type of solution sought after (one could cite for instance time integration, harmonic balance, or perturbation method). However, the analysis of complex systems containing several elements is more challenging. This is already true in the linear domain for which matrix-based methods such as the dynamic stiffness approach [10] or more recently the reverberation ray matrix [11] have been widely used; but the difficulty increases with nonlinearities as one needs to correctly predict the nonlinear interaction between elements. The most common solution is then to use a nonlinear FE model, yet it often becomes computationally expensive if many different meshes need to be generated when performing optimization studies. In contrast, the wave-based approach considered in this paper not only allows the nonlinear vibrational response to be determined efficiently, but also allows the geometry and size of the structure to be varied easily for optimization purposes.

In the linear domain, the principle behind the presented approach, called "ray tracing method", was presented in details in Ref. [12] for a ring-based MEMS gyroscope, and recently used, among others, in Ref. [13] for the analysis of a ring with varying cross-section. It relies on a compact and systematic matrix-based methodology to solve for natural frequencies, mode shapes and harmonically forced response of complex beam-like structures such as multi-span beams or trusses. This approach is exact in a sense that there is no approximation brought by discretization (unlike with Rayleigh-Ritz, modal approach, or FE analysis). It is particularly well suited for the analysis of structures in the high frequency domain where an FE analysis with a mesh too coarse would not be able to separate close modes. Similar wave approaches were used for instance to study the transmission and reflection of waves, or power flow, between Euler-Bernoulli beams [14,15] and later in Timoshenko beams [16,17], and standing waves in a spinning Timoshenko beam [18]. They were developed from the original work of Graff [19] and Cremer et al. [20] who in the first place used the phase-closure, or wave-train closure, principle to derive natural frequencies and mode shapes. More recently, hybrid approaches that consider both an FE model and wave propagations properties, like the wave finite element method, have been broadly considered to model periodic structures (see for instance [21,22]).

As mentioned earlier, some practical engineered structures inherently operate in the nonlinear regime. The literature regarding nonlinear vibrations in beam structures modeled with a wave approach is more succinct. Vakakis [23] first studied the influence of local nonlinearities on wave propagation and showed that an incident wave on a nonlinear boundary generates reflected waves with frequencies equal to multiples of the frequency of the incident wave. Brennan et al. [24] calculated the reflection coefficients and associated power of waves impinging on a cubic hardening or softening spring situated at the end of an infinite beam or rod. They however assumed that the nonlinear effect is relatively weak so that the reflected waves are predominantly at the same frequency of the incident wave, which is equivalent to make a mono-harmonic approximation of the solution.

The objective of the current paper is to develop a methodology to analyse the nonlinear vibrational response of a complex waveguide structure (with several elements). For this purpose, the proposed methodology takes account of the conclusions drawn by Vakakis [23], namely that a wave impinging on a nonlinearity creates different harmonics, and extends the wave approach developed in Ref. [12] for beam-like network to nonlinear vibrations. This work can also be seen as the extension of [24] to a multi-harmonic approach applied to structures with several elements. The originality of the formulation consists in expressing the displacements in any element of the structure as a sum of waves associated with the fundamental frequency and its harmonics. It is an approach similar to the Harmonic Balance (HB) method where the steady state solution of the problem is assumed as a multi-harmonic periodic solution. Instead of using, as more classically performed, the nodal degrees of freedom of an FE model projected into a Fourier basis as unknowns, one here uses the projection of the waves amplitudes.

The manuscript is organized as follows. Section 2 recalls the fundamental existing methodology for linear vibration. Its extension to nonlinear vibrations is presented in details in Section 3 on a simple example, and then generalized to complex beam-like networks in Section 4. The numerical applications in Section 5 validate the proposed approach, demonstrate its efficiency, and show potential uses on a practical application consisting of a representative model of a turbine blade with underplatform friction dampers.

2. Vibration analysis using a wave approach

In this section, we recall the general wave approach formulation used in Ref. [12] for the study of linear vibrations in Euler-Bernoulli beams. The main objective of this paper is to extend this formulation to take account of nonlinear vibrations.

It is assumed that the entire structure is composed of waveguide elements connected and coupled at discontinuities to create a beam-like network. The joints can eventually include the effect of local masses, springs and dampers. The periodic steady state motion of the structure, harmonically vibrating at frequency ω, is defined by expressing the displacement in each element with a sum of waves traveling in opposite directions. The fundamental methodology of the wave approach considered is to assemble matrices that define the travel (propagation and decay) and scattering (transmission and reflection) of these waves through the structure. The effects of wave travel are expressed in a diagonal matrix $\boldsymbol{D}$ called the dispersion matrix. The waves scattering at discontinuities between two or more different elements and the waves reflection at boundaries are expressed by an overall transmission/reflection matrix $\boldsymbol{T}$. The wave amplitudes for all the elements in the positive and negative directions are contained in a vector $\boldsymbol{a}$. This vector $\boldsymbol{a}$ defines the steady state motion of the entire structure. It is solution of [12,25]:

$$\boldsymbol{a} = (\boldsymbol{I} - \boldsymbol{TD})^{-1} \boldsymbol{a}_F^{\text{lin}}, \tag{1}$$

or equivalently:

$$\boldsymbol{a} = \boldsymbol{TDa} + \boldsymbol{a}_F^{\text{lin}}, \tag{2}$$

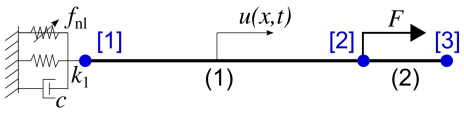

Fig. 1. Bar supported by a linear spring, a linear damper and a nonlinear force.

where $\boldsymbol{I}$ is the identity matrix. The vector $\boldsymbol{a}_F^{\text{lin}}$[1] takes account of the waves generated by the external forces.

Equation (1) can be proved by considering the fact that the steady state is defined with the sum of all the waves present in the structure after an infinite number of ray traces (one ray trace being defined as a single travel and transmission/reflection of the waves). As an equivalent formulation, Eq. (2) stipulates that the steady state solution occurs when the set of wave amplitudes leaving discontinuities in the system is strictly equal to the same set after one ray trace supplemented with the waves created by the external forces.

In Eqs. (1) and (2), the overall unknown wave amplitudes vector $\boldsymbol{a}$ contains waves originating from boundaries or other discontinuities and from excitation forces that must be applied at joints. As it will be presented in Sections 3 and 4, the new formulation proposed in this paper allows to reduce the number of unknowns in the model by solving only for the wave amplitudes at boundaries and discontinuities.

For free vibration analysis, the linear modes are found by setting $\boldsymbol{a}_F^{\text{lin}} = 0$ in (2). The natural frequencies are obtained by solving (generally via numerical means) the characteristic equation $|\boldsymbol{I} - \boldsymbol{TD}| = 0$. Associated mode shapes can be determined by back-substituting the frequency solutions in the $\boldsymbol{T}$ and $\boldsymbol{D}$ matrices of the autonomous system and calculating the corresponding wave amplitudes vector $\boldsymbol{a}$. The wave amplitudes solution are then used in the displacement definition to determine the mode shapes.

In order to extend this wave approach formulation to cope with nonlinear vibrations, the following Section 3 will present an illustrative case of a bar attached to a nonlinear boundary. The generalization of the approach to a beam-like network with local nonlinearities will be made in Section 4.

3. The wave approach to model nonlinear vibrations: illustrative example on a single bar

In this section, we study a bar vibrating longitudinally and attached to a nonlinear boundary. This case study will serve as an example to introduce and explain the innovative formulation of the paper.

3.1. Presentation of the system and the wave formulation

The bar is attached with a combination of linear spring (stiffness k_1), linear viscous damper (coefficient c), and nonlinear restoring force f_{nl} at its left end, and free at its right end. The exciting force is located at a distance L from the left boundary and l from the right one. The presence of the point force divides the initial bar in 2 elements, one on each side of the force. These elements are named (1) and (2) and are defined between the nodes [1], [2], and [3] that correspond to the left boundary, the force application point and the right boundary. The structure is depicted in Fig. 1.

The external excitation force is written on a Fourier basis and can be multi-harmonic. It is composed of harmonic terms F_p of fundamental frequency ω and its multiples, supplemented by a static term F_0. The complex form, with c.c the complex conjugate, is used to defined the force phasing. The external force is written as:

$$F = F_0 + \frac{1}{2}\sum_{p=1}^{N_{hF}} \left(F_p\, e^{\mathrm{i}p\omega t} + \text{c.c} \right). \tag{3}$$

F is a real time-dependent value equal to $F_0 + \sum_{p=1}^{N_{hF}} \left(\Re(F_p)\cos(p\omega t) - \Im(F_p)\sin(p\omega t) \right)$, where $\Re(\bullet)$ and $\Im(\bullet)$ denote respectively the real and imaginary parts. N_{hF} is the number of harmonics used to express the external force in its Fourier decomposition.

The new formulation that forms the basis of the paper relies on the following particular displacement definition. The steady state longitudinal displacement in each element is assumed to be periodic and multi-harmonic with fundamental frequency ω. It is expressed as the sum of a static term (or offset) defined with classical shape functions $N_i^l(x)$ (see Appendix A) of a Euler-Bernoulli beam vibrating longitudinally, and multi-harmonic terms expressed on a Fourier basis defined with forward and backward traveling waves at different speeds. In each element (m) whose ends are node [i] and node [j], the longitudinal displacement noted $u^{(\text{m})}$ is sought after under the form:

$$u^{(\text{m})}(x,t) = \sum_{i=1}^{2} U_i^{(\text{m})} N_i^l(x) + \frac{1}{2}\sum_{p=1}^{N_h} \left(\left(\hat{u}_p^{(\text{m})+} e^{-\mathrm{i}pk_l x} + \hat{u}_p^{(\text{m})-} e^{\mathrm{i}pk_l (x - L^{(\text{m})})} \right) e^{\mathrm{i}p\omega t} + \text{c.c} \right). \tag{4}$$

[1] The superscript "lin" refers to linear as the definition of the external force effects for the nonlinear case will be slightly different, see Sections 3 and 4.

In Eq. (4), x is a local coordinate that varies between 0 and $L^{(\mathrm{m})}$, with $L^{(1)} = L$ for the first element and $L^{(2)} = l$ for the second one. $\hat{u}_p^{(\mathrm{m})\pm}$ is the wave amplitude initiated on the left or right hand side of element (m) and traveling in the positive or negative x direction. k_l is the wavenumber associated with the fundamental frequency ω. For longitudinal vibrations, the wavenumber is $k_l = \omega\sqrt{\rho/E}$ with ρ the bar material density and E its Young's modulus. The pth-harmonic wave has a wavenumber equal to pk_l. The static displacements at node [i] and [j] are respectively $U_1^{(\mathrm{m})}$ and $U_2^{(\mathrm{m})}$. N_h is the number of harmonics retained to express the displacement. It must be greater or equal to N_{hF}. For the sake of simplicity, we will use $N_{hF} = N_h$ in the rest of the development.

The second line of Eq. (4) is in some ways similar to the HB used in FE analysis in which the nodal degrees of freedom are sought after as multi-harmonic periodic solutions. In order to get an algebraic form of the equations that characterize the motion of the structure, as performed in a classical HB procedure, each characteristic equation will be orthogonalized with respect to the basis $\{e_p\}$ where $e_0 = 1$ and $e_p = e^{\mathrm{i}p\omega t}\ \forall p \in [\![1, N_h]\!]$, by means of the inner product defined by Eq. (5), where $\overline{\bullet}$ denotes the complex conjugate.

$$< f, g >= \frac{2}{T}\int_0^T f(t)\overline{g(t)}\,\mathrm{d}t, \quad \text{with} \quad T = \frac{2\pi}{\omega} \tag{5}$$

As the basis function are orthogonal for the chosen scalar product, it simplifies the expression of the projected equations.

3.2. Effects of discontinuities

The equations characterizing each discontinuity are detailed in this section. In each of them, the displacement definition (4) is inserted prior to applying the projection defined in Eq. (5) (details can be found in Appendix B). These projected equations will be rearranged as a fundamental vector equation of motion in Section 3.3.

Left boundary. The left boundary condition is the following force equilibrium:

$$N^{(1)} = k_1 u^{(1)} + c\dot{u}^{(1)} + f_{\mathrm{nl}}^{[1]} \tag{6}$$

taken at $x = 0$ on the first element, where $N^{(1)}$ is the internal tensile force defined as

$$N^{(1)} = EA\frac{\partial u^{(1)}}{\partial x},$$

with A the bar cross-section area. The term $f_{\mathrm{nl}}^{[1]}$ is here the evaluation of the nonlinear boundary condition at node [1] ($x = 0$), and is in a general way function of $(u, \dot{u})$. Using the current formulation, it is function of the unknown static displacement $U_1^{(1)}$, and of the unknown waves amplitudes at the left boundary (created waves amplitudes $\hat{u}_p^{(1)+}$ and incident waves amplitudes $\hat{u}_p^{(1)-}\, e^{-\mathrm{i}pk_lL}$) that define the displacement and velocity of node [1].

Right boundary. At the right boundary, the beam is free to vibrate and the boundary condition is simply

$$N^{(2)} = 0 \tag{7}$$

taken at $x = l$ on the second element.

Point force. At the application point of the force, the system must respect displacement continuity. This is expressed in Eq. (8a). The external force also generates new waves within the structure originating from its application point. The force equilibrium taken at this point (in $x = L$ for element (1) and $x = 0$ for element (2)) gives Eq. (8b).

$$u^{(1)}(L, t) = u^{(2)}(0, t) \tag{8a}$$

$$F = N^{(1)} - N^{(2)} \tag{8b}$$

Combining the projections of the conditions expressed in (8) gives the following relationships that link the waves at the application point of the force and the waves at the boundaries: $\forall p \in [\![1, N_h]\!]$,

$$\hat{u}_p^{(1)-} = \hat{u}_p^{(2)-}\, e^{-\mathrm{i}pk_l l} + \frac{F_p}{2\mathrm{i}EApk_l} \tag{9a}$$

$$\hat{u}_p^{(2)+} = \hat{u}_p^{(1)+}\, e^{-\mathrm{i}pk_l L} + \frac{F_p}{2\mathrm{i}EApk_l} \tag{9b}$$

3.3. Equation of motion

3.3.1. Static term

The static term of the equation of motion is found by combining the projections on $e_0 = 1$ of the conditions describing the discontinuities detailed in Section 3.2. It can be written under the form:

$$\boldsymbol{K}_0\boldsymbol{a}_0 + \boldsymbol{f}_{\mathrm{nl},0} = \boldsymbol{f}_0 \tag{10}$$

The vectors and matrices appearing in the above Eq. (10) are defined next:

- The vector $\boldsymbol{a}_0$ of size 3 contains the unknown nodal static displacements: $\boldsymbol{a}_0 = \begin{bmatrix} U_1^{(1)} & U_2^{(1)} (= U_1^{(2)}) & U_2^{(2)} \end{bmatrix}^{\mathrm{T}}$.
- The matrix $\boldsymbol{K}_0$ is the stiffness matrix of the associated linear system. It corresponds to the standard stiffness matrix of a finite element model with 2 bar elements (length L and l) whose first node is attached to a linear stiffness k_1:

$$\boldsymbol{K}_0 = EA \begin{bmatrix} \frac{1}{L} + \frac{k_1}{EA} & -\frac{1}{L} & 0 \\ -\frac{1}{L} & \frac{1}{L} + \frac{1}{l} & -\frac{1}{l} \\ 0 & -\frac{1}{l} & \frac{1}{l} \end{bmatrix}$$

- The vector of external static force $\boldsymbol{f}_0$ defines the forces applied to each node. It is in our example equal to $\boldsymbol{f}_0 = \begin{bmatrix} 0 & F_0 & 0 \end{bmatrix}^{\mathrm{T}}$.
- The vector of nonlinear static forces $\boldsymbol{f}_{\mathrm{nl},0}$ contains the static term of the nonlinear force evaluated at each node obtained by projection with the scalar product $< \bullet, 1 >$. It is here given by $\boldsymbol{f}_{\mathrm{nl},0} = \begin{bmatrix} < f_{\mathrm{nl}}^{[1]}, 1 > /2 & 0 & 0 \end{bmatrix}^{\mathrm{T}}$.

3.3.2. Harmonic terms

The equation of motion that refers to the harmonic terms is found by combining the projections on e_p of the conditions describing the discontinuities detailed in Section 3.2. It can be written under the general form:

$$\boldsymbol{a} = \boldsymbol{T}\left(\boldsymbol{D}\boldsymbol{a} + \boldsymbol{D}_F\boldsymbol{a}_F\right) - \boldsymbol{f}_{\mathrm{nl}}. \tag{11}$$

The vectors and matrices appearing in the above Eq. (11) are defined next. In the following, the index p takes values from 1 to N_h.

- The unknown wave amplitudes at the left and right boundaries of the beam are contained in a single vector $\boldsymbol{a}$ of size $2N_h$:

$$\boldsymbol{a} = \begin{bmatrix} \boldsymbol{a}^{(1)+} \\ \boldsymbol{a}^{(2)-} \end{bmatrix},$$

  where $\boldsymbol{a}^{(1)+} = \begin{bmatrix} \dots & \hat{u}_p^{(1)+} & \dots \end{bmatrix}^{\mathrm{T}}$ and $\boldsymbol{a}^{(2)-} = \begin{bmatrix} \dots & \hat{u}_p^{(2)-} & \dots \end{bmatrix}^{\mathrm{T}}$.
- The linear transmission/reflection matrix $\boldsymbol{T}$ is given by:

$$\boldsymbol{T} = \begin{bmatrix} \boldsymbol{0} & \boldsymbol{T}_{\mathrm{left}} \\ \boldsymbol{T}_{\mathrm{right}} & \boldsymbol{0} \end{bmatrix},$$

  where the left and right linear reflection matrices ($\boldsymbol{T}_{\mathrm{left}}$ and $\boldsymbol{T}_{\mathrm{right}}$) are diagonal matrices whose pth components (T_{left} and T_{right}) are:

$$T_{\mathrm{left}} = \frac{-k_1 + \mathrm{i}p(-c\omega + EAk_l)}{k_1 + \mathrm{i}p(c\omega + EAk_l)} \quad \text{and} \quad T_{\mathrm{right}} = 1.$$

- The dispersion matrix $\boldsymbol{D}$ accounts for the propagation of the waves along the total length of the beam ($L + l$) and is given by:

$$\boldsymbol{D} = \begin{bmatrix} \boldsymbol{\Delta}(L+l) & \boldsymbol{0} \\ \boldsymbol{0} & \boldsymbol{\Delta}(L+l) \end{bmatrix}.$$

  $\boldsymbol{\Delta}(L^{(\mathrm{m})})$ is a diagonal matrix that defines the propagation of waves along an element of length $L^{(\mathrm{m})}$. Its pth term is $e^{-\mathrm{i}pk_lL^{(\mathrm{m})}}$. The pth term of $\boldsymbol{\Delta}(L + l)$ is therefore equal to $e^{-\mathrm{i}pk_l(L+l)}$.
- The wave amplitudes vector $\boldsymbol{a}_F$ refers to the waves created by the external force and that propagate away from its application point:

$$\boldsymbol{a}_F = \begin{bmatrix} \boldsymbol{a}_F^{(2)+} \\ \boldsymbol{a}_F^{(1)-} \end{bmatrix}$$

where in this particular case (case of a tensile external point force) the wave amplitude propagating in the negative direction is equal to the one propagating in the positive direction $\boldsymbol{a}_F^{(1)-} = \boldsymbol{a}_F^{(2)+}$. Their pth-component is $F_p/(2\mathrm{i}EApk_l)$.

- The dispersion matrix $\boldsymbol{D}_F$ refers to the propagation of the waves created by the external forces. The right hand side waves propagate in element (2) (length l), whereas the left hand side waves propagate in element (1) (length L):

$$\boldsymbol{D}_F = \begin{bmatrix} \boldsymbol{\Delta}(l) & \boldsymbol{0} \\ \boldsymbol{0} & \boldsymbol{\Delta}(L) \end{bmatrix}.$$

- The vector $\boldsymbol{f}_{\mathrm{nl}}$ characterizes the nonlinear effect occurring at the bar boundaries. The bar boundaries are at nodes [1] and [3]. This effect is function of the displacement and velocity of the boundary nodes. $\boldsymbol{f}_{\mathrm{nl}}$ is therefore function of created waves $\boldsymbol{a}$, incident waves at boundaries $\boldsymbol{Da} + \boldsymbol{D}_F\boldsymbol{a}_F$, and static displacements $U_1^{(1)}$ and $U_2^{(2)}$. It takes the general form:

$$\boldsymbol{f}_{\mathrm{nl}} = \begin{bmatrix} \boldsymbol{f}_{\mathrm{nl}}^{[1]} \\ \boldsymbol{f}_{\mathrm{nl}}^{[3]} \end{bmatrix}.$$

In the current example, the right boundary is linear so $\boldsymbol{f}_{\mathrm{nl}}^{[3]} = \boldsymbol{0}$, whereas the left boundary contains a nonlinear restoring force $f_{\mathrm{nl}}^{[1]}$ and then $\boldsymbol{f}_{\mathrm{nl}}^{[1]}$ is given by:

$$\boldsymbol{f}_{\mathrm{nl}}^{[1]} = \begin{bmatrix} \vdots \\ \dfrac{< f_{\mathrm{nl}}^{[1]},\, e^{\mathrm{i}p\omega t} >}{k_1 + \mathrm{i}p(c\omega + EAk_l)} \\ \vdots \end{bmatrix}.$$

Equation (11) can be simplified to the linear equation (2) by suppressing all nonlinear effects and keeping only the fundamental harmonic term in the displacement definition ($\hat{u}_p^{(\mathrm{m})\pm} = 0, \forall p > 1$). However, in Eq. (11), even for linear simulation, the number of unknowns has been reduced compared to (2) by substituting the term $\boldsymbol{a}_F^{\mathrm{lin}}$ with $\boldsymbol{TD}_F\boldsymbol{a}_F$ which directly accounts for the external forcing without introducing new variables (the waves created at node [2] do not directly appear in the vector of unknowns $\boldsymbol{a}$, which would not have been the case with the formulation of Eq. (2)).

3.3.3. *General equation of motion*

Equations (10) and (11) can be combined in a general algebraic form by defining a single vector $\widehat{\boldsymbol{x}}$ that contains all the unknowns of the problem:

$$\boldsymbol{Z}(\omega)\widehat{\boldsymbol{x}} + \widehat{\boldsymbol{f}}_{\mathrm{nl}}(\widehat{\boldsymbol{x}}, \omega) = \boldsymbol{f}_{\mathrm{ext}}(\omega). \tag{12}$$

where

$$\widehat{\boldsymbol{x}} = \begin{bmatrix} \boldsymbol{a}_0 \\ \boldsymbol{a} \end{bmatrix}, \quad \boldsymbol{Z} = \begin{bmatrix} \boldsymbol{K}_0 & \boldsymbol{0} \\ \boldsymbol{0} & \boldsymbol{I} - \boldsymbol{TD} \end{bmatrix}, \quad \widehat{\boldsymbol{f}}_{\mathrm{nl}} = \begin{bmatrix} \boldsymbol{f}_{\mathrm{nl},0} \\ \boldsymbol{f}_{\mathrm{nl}} \end{bmatrix} \quad \text{and} \quad \boldsymbol{f}_{\mathrm{ext}} = \begin{bmatrix} \boldsymbol{f}_0 \\ \boldsymbol{TD}_F\boldsymbol{a}_F \end{bmatrix} \tag{13}$$

$\boldsymbol{I}$ is the identity matrix of size $2N_h$. The vector of unknowns $\widehat{\boldsymbol{x}}$, of size $2N_h + 3$, defines both the nodal static displacements and the multi-harmonic waves amplitudes. The matrix $\boldsymbol{Z}$ is a multi-harmonic dynamic stiffness matrix and is function of the excitation frequency ω via matrices $\boldsymbol{T}$ and $\boldsymbol{D}$. The external force is considered via the vector $\boldsymbol{f}_{\mathrm{ext}}$ that basically defines the static force on each node, and the created waves amplitude after propagation along an element and reflection at the boundary. The nonlinear effect is defined with $\widehat{\boldsymbol{f}}_{\mathrm{nl}}$; it contains the projection of the evaluation of the nonlinear force on each harmonic.

For a given excitation frequency ω, the nonlinear algebraic equation (12) can be solved with classic iterative algorithm such as the Newton-Raphson method. However, as the wave amplitudes in $\widehat{\boldsymbol{x}}$ are complex, one needs first to decompose it with its real and imaginary part. The total number of unknowns in the problem is therefore $4N_h + 3$. The steady state displacement in each element is then found by substituting part of the solution of (12) in Eq. (9) and subsequently substituting the wave amplitudes in Eq. (4).

As the entire formulation is in complex form, it is straightforward to include hysteretic damping in the system using a complex Young's modulus equal to $E(1 + \mathrm{i}\eta)$, where η is the loss factor, instead of the real Young's modulus of the material. This damping modeling will be used in the applications presented in Section 5.

4. Generalization: the nonlinear wave formulation for a beam-like network

The objective of this section is to generalize the formulation presented in the case of the nonlinear vibrations of a single bar in Section 2 to the case of nonlinear vibrations of a beam-like network with any number of elements. It focuses on the main differences between the linear and the nonlinear approaches, and on the size of the obtained problem.

The beam-like network considered is a structure that consists of N_{el} beam elements connected between each other at N_{nd} joints or nodes. Fig. 2 illustrates an example with $N_{\mathrm{el}} = 8$ and $N_{\mathrm{nd}} = 8$. Point forces must be applied at nodes. We consider

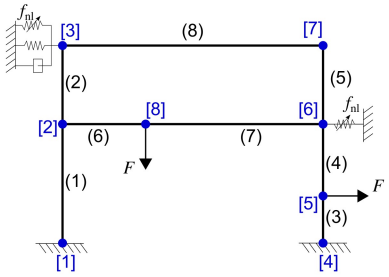

Fig. 2. Example of a beam-like network with localized nonlinearities.

in this paper only in-plane vibrations of straight Euler-Bernoulli beam elements but the extension to Timoshenko beams, out-of-plane vibrations, or curved beams elements should be relatively straightforward following the explanation in Refs. [16,25] developed for linear vibrations.

The fundamental difference with the linear approach is that the displacement in each element is defined with a sum of a static term and a multi-harmonic term that refers to waves vibrating at the fundamental frequency and its harmonics. Thanks to this wave formulation, detailed in the next section, the vibrational motion of the system is characterized with an algebraic equation that takes the same form as Eq. (12) whatever the number and type of elements. The evaluation of the nonlinear effects on the wave reflection/transmission is also an innovative aspect of the paper that deserves particular attention.

4.1. Displacement formulation and wave propagation

In each element (m), $\mathsf{m} \in [\![1, N_{\text{el}}]\!]$, connected between node [i] and [j], $\mathsf{i}, \mathsf{j} \in [\![1, N_{\text{nd}}]\!]$, the longitudinal and transverse displacements are expressed in a local frame attached to the element (m), where x runs from 0 to the length $L^{(\mathsf{m})}$ of the element. The longitudinal displacement $u(x,t)$ is defined as in Eq. (4). The transverse displacement $v(x,t)$ definition incorporates near field waves:

$$v^{(\mathsf{m})}(x,t) = \sum_{i=1}^{4} V_i^{(\mathsf{m})} N_i^f(x) + \frac{1}{2}\sum_{p=1}^{N_h} \left(\left(\hat{v}_p^{(\mathsf{m})+} e^{-\mathrm{i}\sqrt{p}k_f x} + \hat{v}_p^{(\mathsf{m})-} e^{\mathrm{i}\sqrt{p}k_f (x-L^{(\mathsf{m})})} + \hat{w}_p^{(\mathsf{m})+} e^{-\sqrt{p}k_f x} + \hat{w}_p^{(\mathsf{m})-} e^{\sqrt{p}k_f (x-L^{(\mathsf{m})})} \right) e^{\mathrm{i}p\omega t} + \text{c.c} \right). \tag{14}$$

In Eq. (14), the shape functions N_i^f ($i = 1$ to 4) are classical shape functions defining the transverse displacement of a Euler-Bernoulli beam element and are recalled in Appendix A. They are associated with $V_i^{(\mathsf{m})}$ the transverse displacement and slope at node [i] and [j]. $\hat{v}_p^{(\mathsf{m})\pm}$ and $\hat{w}_p^{(\mathsf{m})\pm}$ are the wave amplitudes of propagating and decaying (near field) waves for flexural vibration, initiated on the left or right hand side of element (m), traveling in the positive or negative x direction. The wavenumber for flexural vibration associated with the fundamental frequency ω is $k_f = \sqrt{\omega\sqrt{\rho A/(EI)}}$, where I is the second moment of area of the cross section. The pth-harmonic wave, with frequency $p\omega$, has a wavenumber equal to $\sqrt{p}k_f$.

All of the waves amplitudes (longitudinal $\hat{u}_p^{(\mathsf{m})\pm}$ of Eq. (4), flexural propagating $\hat{v}_p^{(\mathsf{m})\pm}$ of Eq. (14) and flexural decaying $\hat{w}_p^{(\mathsf{m})\pm}$ of Eq. (14)) are contained in the overall vector $\boldsymbol{a}$ of the general equation of motion (12). The number of waves amplitudes unknown is $6N_hN_{\text{el}}$ (3 waves per harmonic propagating in the positive direction and negative directions of each element). The size of $\boldsymbol{a}$ is not necessarily $6N_hN_{\text{el}}$ because it depends on the number of point forces that are applied within a beam (this excludes point force at corners or any other discontinuity). The waves leaving the point forces are not direct unknowns and appear in the forcing term (right-hand side of Eq. (12)) vector $\boldsymbol{a}_F$. Relationships similar to the ones in Eq. (9) can be used as post-processing to calculate the waves leaving the point force and then derive the waves at each end of all elements. The vector $\boldsymbol{a}$ is therefore of size $6N_hN_{\text{el}}^{\text{free}}$ (with $N_{\text{el}}^{\text{free}} \leq N_{\text{el}}$) where $N_{\text{el}}^{\text{free}}$ is the minimal number of elements of the structure in the autonomous case. For instance, $N_{\text{el}}^{\text{free}} = 1$ for the structure illustrated in Fig. 1, $N_{\text{el}}^{\text{free}} = 6$ for the one in illustrated in Fig. 2, and $N_{\text{el}}^{\text{free}} = 2$ for the one in Fig. 4 or Fig. 9b.

In order to cope with possible offset created by nonlinear forces (for instance from a quadratic force) and also to consider the possibility of a constant external force, static terms were added in the formulation compared to Eq. (2). Those are included in vector $\boldsymbol{a}_0$ of Eq. (12) that contains the terms $U_i^{(\mathsf{m})}$ of Eq. (4) and $V_i^{(\mathsf{m})}$ of Eq. (14). $\boldsymbol{a}_0$ defines the displacement in two directions and slope of the structure at nodal points. The size of $\boldsymbol{a}_0$ is simply $3N_{\text{nd}}$ because each node has got 3 degrees of freedom (for in-plane displacement). In the final characteristic equation to solve, Eq. (12), these terms are multiplied by a global static stiffness matrix $\boldsymbol{K}_0$. This global stiffness matrix is found by assembling elementary stiffness matrices, as in a classical FE procedure. $\boldsymbol{K}_0$ must take account of an eventual change of frame from a rotated local frame associated with the element to a global frame. It must also contain the stiffness value of any linear spring added to the structure.

Vector $\boldsymbol{a}_F$ of Eq. (12) contains the waves amplitudes created by the external point forces. The derivation of those waves amplitudes is given in Section 3 for an external longitudinal force and in Ref. [25] for external tangential force and moment. The size of $\boldsymbol{a}_F$ is $6N_h(N_{\text{el}} - N_{\text{el}}^{\text{free}})$.

The waves amplitudes vector $\boldsymbol{a}$ is multiplied by the dispersion matrix $\boldsymbol{D}$ in Eq. (12) to take account of the waves travel, change of phase and decay. $\boldsymbol{D}$ is a square diagonal matrix which contains the terms $e^{-\mathrm{i}pk_l L}$, $e^{-\mathrm{i}\sqrt{p}k_f L}$ and $e^{-\sqrt{p}k_f L}$ in association with the waves amplitudes $\hat{u}_p^{(\mathrm{m})\pm}$, $\hat{v}_p^{(\mathrm{m})\pm}$ and $\hat{w}_p^{(\mathrm{m})\pm}$ respectively. The length L is the length of the beam on which the waves can travel in the autonomous case without encountering a discontinuity. It is equal to $L^{(\mathrm{m})}$ except when the wave impinges on an isolated point force.

Similar terms are contained in the matrix $\boldsymbol{D}_F$ which accounts for the propagation of waves created by the external forces. The waves propagate in the positive and negative directions, starting from the point forces and up to the next discontinuities (or nodes). $\boldsymbol{D}_F$ is generally not a square matrix and its size is $6N_h N_{\text{el}}^{\text{free}} \times 6N_h(N_{\text{el}} - N_{\text{el}}^{\text{free}})$.

It may be important to recall at this point that the waves amplitudes are complex values. By consequence the real number of unknowns to solve in the nonlinear algebraic system of equation (12) is twice the length of $\boldsymbol{a}$ added to the number of static nodal degrees of freedom, i.e. $12N_h N_{\text{el}}^{\text{free}} + 3N_{\text{nd}}$.

4.2. Transmission/reflection at discontinuities

As in the linear case recalled in Section 2, the main difficulty of this matrix-based wave approach relies on having knowledge of the detailed transmission characteristics of waves at discontinuities of the structure. The methodology to derive the transmission coefficient of any number of beam elements connected to a linear joint was explained in Ref. [25]. The overall linear transmission matrix $\boldsymbol{T}$ is constructed by accounting for the equations characterising displacement and slopes continuities, and force and moment equilibrium, at the different linear discontinuities in the system taken independently from each other. With the displacements formulated using Eqs. (4) and (14), $\boldsymbol{T}$ contains terms that generally depend of the harmonic considered.

At discontinuities where linearities and nonlinearities are combined, the linear and nonlinear effects must be separated. The linear part is incorporated in the $\boldsymbol{T}$-matrix whereas the nonlinear part is kept as general as possible in the form of $< f_{\text{nl}}, e^{ip\omega t} >$ and accounted for in the $\widehat{\boldsymbol{f}_{\text{nl}}}$ vector of Eq. (12). f_{nl} is generally function of the displacement and velocity of the nodes. It can take different forms depending on the type of nonlinearity (Duffing, friction, impact, etc.). These nonlinear discontinuities can be either boundaries (see for instance the models illustrated in Figs. 1 and 4) or intermediate supports (such as illustrated in Figs. 2 and 9b). The vector $\widehat{\boldsymbol{f}_{\text{nl}}}$ has got the same size as $\widehat{\boldsymbol{x}}$ and contains non-zero values only on components associated with the nodes on which a nonlinearity is attached (for instance nodes [3] and [6] in Fig. 2).

4.3. Projection of the nonlinear force onto the Fourier basis

In some cases, for instance when N_h is relatively small and the nonlinear force writes as a polynomial function, it is easy to develop an analytical formulation of $\widehat{\boldsymbol{f}}_{\text{nl}}$, which contains the projection of the nonlinear force onto the Fourier basis. However, in practical applications, an analytical expression of $\widehat{\boldsymbol{f}}_{\text{nl}}$ might be cumbersome to obtain depending on the nature of the nonlinearity.

This nonlinear term is instead determined numerically through an alternate frequency-time (AFT) scheme [26] that must be performed at each iteration of the solver. This scheme was for instance used in Refs. [27–29], and is described in the following. Starting with a guess on the $\widehat{\boldsymbol{x}}$-value, a direct discrete Fourier transform is performed on $\widehat{\boldsymbol{x}}$. By this mean, the wave amplitudes and therefore the displacement and velocity in the structure are sampled in the time domain at equidistant time points within one period of oscillation. These displacements and velocities are evaluated at the location of the nonlinearities and used to compute the nonlinear force in the time domain. Finally an inverse discrete Fourier transform performed on the nonlinear force gives the projection of this force in the frequency domain, which corresponds to an evaluation of $\widehat{\boldsymbol{f}}_{\text{nl}}$. In practice, the sample size retained in this time-discrete AFT scheme is likely to influence the convergence of the solver. It is generally necessary to find a compromise between convergence and computation time, while ensuring that the sampling period satisfies Nyquist-Shannon's theorem.

5. Validation - application

The objective of the first two following applications is to compare the efficiency of the proposed approach with FE simulations. Academic examples are illustrated to cover a broad range of analyses and to show the flexibility and robustness of the wave approach. In the last application, Section 5.3, a simplified model of a turbine blade with friction dampers is considered and results are compared with those obtained from numerical time integration. The transmission/reflection coefficients of the different discontinuities encountered are also detailed.

In the following FE simulations, the solutions of the nonlinear equation of motions are found using a classical HB procedure, in which the nodal solution is written as a Fourier series truncated to an order N_h. For the sake of coherent comparison between

the two approaches, the same number of harmonic is used when a direct comparison is made. It is not the purpose of this current work to prove the convergence with respect to N_h for a general case. Furthermore, in order to compute continuous frequency response functions and overcome possible turning points when solving Eq. (12), an arc-length continuation algorithm with tangent prediction step [30] is used. The frequency ω is considered as a variable of the problem along with the Fourier coefficient. The evaluation of the nonlinear terms in the frequency domain is performed through the AFT scheme using the same temporal discretization in the Discrete Fourier Transform in both FE and wave approach simulations.

5.1. Simple bar with a nonlinear boundary

5.1.1. Free vibration analysis

In this section we demonstrate the validity of the wave formulation presented in Section 3 on very simple cases by comparison with analytical results from the literature. These are the free linear and nonlinear analyses of a bar (length L) when it is extremely rigid and assumed to act as a rigid mass. We here assume that the nonlinear force is a restoring cubic force with stiffness k_3. This force is defined as $f_{\text{nl}} = k_3 u^3$ at $x = 0$.

The system studied is the bar illustrated in Fig. 1. The development made in Section 3 is used and will be simplified, when needed, with different hypotheses. In the autonomous conservative case ($F = 0$ and $c = 0$) and by keeping only one harmonic in Eq. (4) to represent the steady state solution, Eq. (12) reduces to:

$$\left(1 - \frac{-k_1 + \mathrm{i}EAk_l}{k_1 + \mathrm{i}EAk_l}\, e^{-2\mathrm{i}k_l L}\right) \hat{u}_1^+ + \frac{3k_3}{4(k_1 + \mathrm{i}EAk_l)} \left(\hat{u}_1^+ (1 + e^{-2\mathrm{i}k_l L})\right)^2 \left(\bar{\hat{u}}_1^+ (1 + e^{2\mathrm{i}k_l L})\right) = 0. \tag{15}$$

In the autonomous case and with $l = 0$, there is no distinction between element (1) and (2) so the notation has been simplified accordingly. The nonlinear term of Eq. (15) was obtained by analytically calculating the scalar product $< k_3 u^3_{x=0},\, e^{\mathrm{i}\omega t} >$.

For linear vibrations, the natural frequencies of the system considered are obtained by zeroing the first term of Eq. (15), which reduces to solving:

$$\frac{k_1}{EA} \cos(k_l L) - k_l \sin(k_l L) = 0. \tag{16}$$

An identical expression can be found by a more classical approach where the boundary conditions $EA(\partial u(0,t)/\partial x) = k_1 u(0,t)$ and $EA(\partial u(L,t)/\partial x) = 0$ are applied to get the c_1 and c_2 values of the general form of displacement $u(x,t) = (c_1 \cos(kx) + c_2 \sin(kx)) \sin(\omega t)$. In the case of an extremely rigid bar ($E \to \infty$), Eq. (16) gives $k_l^2 = k_1/(EAL)$, equivalent to $\omega^2 = k_1/(\rho AL)$, which corresponds to the expression of the natural frequency, later called ω_0, of a rigid mass $m = \rho AL$ attached to a linear spring of stiffness k_1.

If the same rigid bar is now supported by nonlinear supports (a cubic stiffness), the nonlinear modes can be obtained with the following expression derived from Eq. (15) with $E \to \infty$:

$$\omega_0^2 - \omega^2 + 3\frac{k_3}{m} \hat{u}_1^+ \bar{\hat{u}}_1^+ = 0. \tag{17}$$

It gives the relationship between the nonlinear natural frequency ω and the amplitude of displacement in the bar (defined with $\hat{u}_1^+$). Nonlinear modes differ from their linear analog in that they are energy-dependent. The displacement definition, Eq. (4), without constant terms, with a single harmonic and when considering $E \to \infty$, is no longer function of x and simplifies to: $u(t) = \hat{u}_1^+ e^{\mathrm{i}\omega t} + \text{c.c.}$ So if one looks for the complex term $\hat{u}_1^+$ in the form $\hat{u}_1^+ = a + \mathrm{i}b$, the displacement becomes $u(t) = 2a\cos(\omega t) - 2b\sin(\omega t)$, and the condition to find the nonlinear mode (Eq. (17)) rewrites as:

$$\omega_0^2 - \omega^2 + \frac{3k_3}{4m} \left((2a)^2 + (2b)^2\right) = 0. \tag{18}$$

This later expression defines the nonlinear mode of a duffing oscillator of mass m and is identical to the one obtained directly by applying a single harmonic approximation on the solution of the fundamental equation $m\ddot{u} + k_1 u + k_3 u^3 = 0$ [31].

5.1.2. Forced vibration analysis

We now consider the bar of Fig. 1 to be excited by a point force $F = F_1 \cos \omega t$. The nonlinear force used is a general polynomial force defined as $f_{\text{nl}} = k_2 u^2 + k_3 u^3$ at $x = 0$. The presence of a quadratic term in $k_2 u^2$ makes its effect non-symmetrical and creates an offset in the harmonic displacement (or constant term). This motivates the use of static terms (U_i for longitudinal and V_i for transverse vibrations) in the proposed formulation. The numerical values used in the following simulations are (notation detailed in Section 3): $N_h = 3, E = 200\,\text{GPa}, \rho = 7850\,\text{kg/m}^3, L = 75\,\text{cm}, l = 25\,\text{cm}$, circular cross-section with diameter 2 cm, $F_1 = 2000\,\text{N}, c = 100\,\text{Ns/m}, k_1 = 6 \times 10^7\,\text{N/m}, k_2 = 1.1 \times 10^{11}\,\text{N/m}^2, k_3 = 10^{14}\,\text{N/m}^3$.

Fig. 3 illustrates the peak-to-peak amplitude of the longitudinal displacement taken at the bar right boundary as a function of the excitation frequency around the second linear mode. The results illustrated were obtained with the proposed wave approach and with FE analyses (supplemented by a HB procedure) for different number of bar elements. The finite elements used are linear 2 nodes bar elements whose shape functions are given in Appendix A. The linear solution (obtained with $k_2 = k_3 = 0$) is also superimposed on the figure. This figure demonstrates that the FE solution converges towards the wave approach solution.

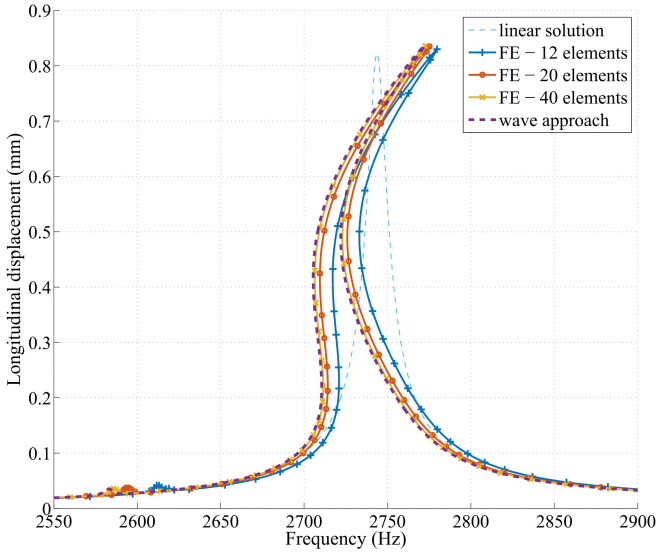

Fig. 3. Longitudinal displacement of a bar with nonlinear boundary conditions under harmonic forcing.

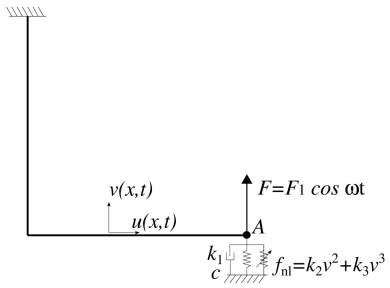

Fig. 4. Beam-like network composed of two elements and supported by a nonlinear force.

As in the linear case, the wave approach solves directly for the exact solution of the governing equations of motion. The FE approximation naturally tends to that "perfect" solution. In this particular simulation, one would need approximately 40 bar elements to obtain a similar accuracy.

The main advantage of the proposed approach lies in its reduction cost. The nonlinear algebraic system to solve obtained from the FE model after an HB procedure is of size $(2N_h + 1)N_{\text{dof}}$[2] (where N_{dof} the number of degrees of freedom in the FE discretization), whereas the wave approach system size is $4N_h + 3$. For instance, with 40 elements and $N_h = 3$, the number of unknowns goes from 287 in the FE analysis to 15 in the wave approach.

5.2. Beam-like network with a nonlinear boundary

The objective of this second example is to demonstrate the generalization of the proposed approach to a complex beam-like network. It is here simply applied to a 2-beams system connected at a right angle but the same assembly and solution methodologies can be used for a larger structure. The system, depicted in Fig. 4, is chosen so that both longitudinal and transverse displacements coexist in the elements. It is clamped in one end, and supported by a linear spring, a linear viscous damper, and a nonlinear polynomial restoring force (with quadratic and cubic terms – similar to the one used in Section 5.1.2) in the other end. The nonlinear boundary is called end '*A*'. The transmission/reflection coefficients of the structure (at its right angle and its end *A*) are given in Appendix C.

A harmonic forcing is exerted in *A* with varying frequency. The structure material is defined with $E = 200\,\text{GPa}$ and $\rho = 7850\,\text{kg/m}^3$; each beam has a length $L = 50\,\text{cm}$ and a rectangular cross-section with in-plane thickness 2 mm and out-of-plane width 2 cm.

Fig. 5 illustrates the peak-to-peak amplitude of the transverse displacement v in A, called v_A, as a function of the exci-

[2] Only because the Young's modulus is here considered as real-valued, otherwise the size would be $(2N_h + 2)N_{\text{dof}}$.

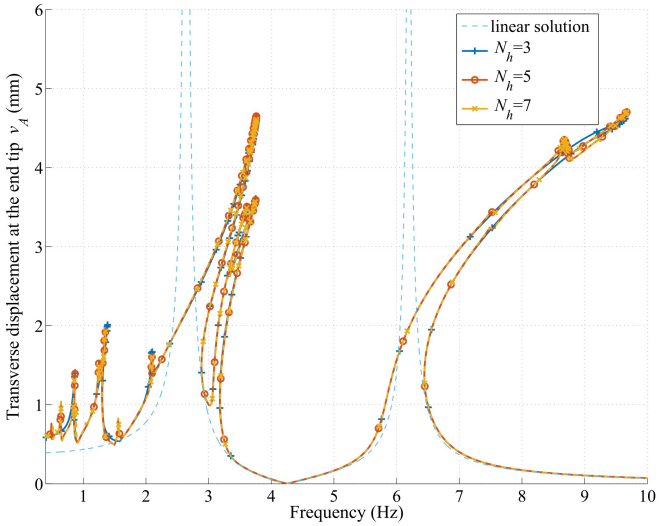

Fig. 5. Transverse displacement at the nonlinear boundary as a function of the excitation frequency; calculated with the wave approach for different number of harmonics retained N_h.

tation frequency around the first two linear natural frequencies. The parameters used are here: stiffnesses $k_1 = 10\,\mathrm{N/m}$, $k_2 = 2 \times 10^4\,\mathrm{N/m^2}$, $k_3 = 10^7\,\mathrm{N/m^3}$, external force $F_1 = 0.01\,\mathrm{N}$, and damping defined only via a complex modulus with loss factor $\eta = 0.01$ (and $c = 0$). The simulations were performed with the proposed wave approach and with different numbers of harmonics (N_h). As expected, it shows that the solution converges when N_h increases. This converges the same way as a classical FE simulation with HB for a given number of elements. For completeness, the linear solution, calculated with $k_2 = k_3 = 0$, is also plotted in Fig. 5.

For a given N_h-value ($N_h = 3$) and using the same system configuration parameters, Fig. 6 shows the amplitude of the transverse (v_A) and longitudinal (u_A) displacements in A as a function of the excitation frequency, calculated with the wave approach and an FE model. The FE results were obtained with 15 Euler-Bernoulli beam elements (whose shape functions are given in Appendix A) in each beam. The responses match perfectly. Furthermore, at the resonant peaks (large black circle and cross in Fig. 6), the mode shapes obtained with the wave approach agree very well with those obtained with the FE analysis, see Fig. 7. This validates the proposed approach for coupled longitudinal/transverse vibrations.

In order to emphasize the advantage of the proposed wave approach, the simulations illustrated in Fig. 8 focus on high frequency response. The excitation frequency is now set around the 21st to 25th linear modes of vibration. Compared to previous simulations of Figs. 5 and 6, some parameters were changed so as to sharpen the results. The new parameters are: stiffnesses

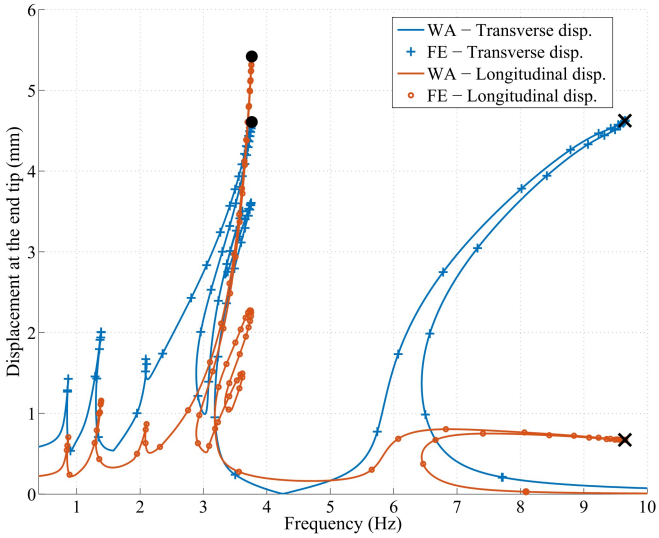

Fig. 6. Displacement in A as a function of the excitation frequency; comparison between the wave approach (WA) and FE simulations.

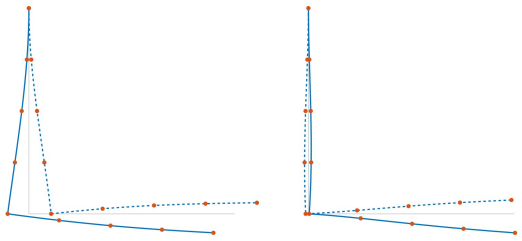

(a) (b)

Fig. 7. Deformed shapes at the first 2 resonant peaks: (a) – 1st mode (black circle in Fig. 6), and (b) – 2nd mode (black cross in Fig. 6). Comparison between the wave approach (deformed extrema are shown with full and doted lines) and an FE simulation (red dots). (For interpretation of the references to colour in this figure legend, the reader is referred to the Web version of this article.)

$k_2 = 5 \times 10^6\,\mathrm{N/m^2}$, $k_3 = 2 \times 10^{11}\,\mathrm{N/m^3}$, external force $F_1 = 200\,\mathrm{N}$, and damping via loss factor $\eta = 0.005$. Fig. 8 compares the displacements in A calculated with an FE analysis and different numbers of elements and the wave approach. It shows that a high number of degrees of freedom (DoF) (at least 273) in the FE analysis is needed to correctly characterize the response of the structure at high frequency. With nonlinear effects, it may become more difficult to separate close modes if the model is not accurate enough. Considering 3 harmonics, the total number of unknowns goes from 2208 in the FE analysis with 273 DoF to 81 in the wave approach. The numerical cost reduction offered by the wave approach is drastic, and this reduction is achieved for a model that is even more accurate than the FE one.

5.3. Simplified model of a turbine blade with underplatform damper

Vibration mitigation of turbine blades is a challenge of great interest as blades are key components that undergo many sources of excitation and risk stress failure. Friction dampers have proved efficient in moderating vibrations and their strong nonlinear effects are now relatively well understood thanks to numerous numerical and experimental investigations (see for instance [27,32–34]). In some situations, the damper can be designed as a blade-to-ground dry friction damper. In contact with the coverplate or the disk, the damper is stationary with respect to the blade, and energy is dissipated through the frictional contact due to the relative motion between the blade and the so-called ground. A schematic representation of such design is illustrated in Fig. 9a.

As an illustrative example to show the capabilities of the proposed wave approach, we study in this section the forced response of a representative model of a blade with an underplatform blade-to-ground damper. The model considered is illustrated in Fig. 9b. The blade is modeled with a cantilever uniform beam excited at its tip. Coulomb's dry friction law is used to model the dissipative nonlinear forces arising from the friction between the blade platform and the ground. The dry friction effect is described with a hyperbolic tangent regularization of the sign function of the Coulomb's law. The associated nonlinear force, function of the velocity of the point in contact $\dot{v}_B$, is written as:

$$f_{\mathrm{nl}}(\dot{v}_B) = \mu N \tanh \frac{\dot{v}_B}{\epsilon}. \tag{19}$$

where μ is the friction coefficient and N represents the normal load enforcing the contact. In practice, this load is mainly due to centrifugal effects and is function of the rotational speed of the blade (see for instance [28] for a parameter study on the influence of the centrifugal force). Both parameters are considered as constant and equal to $\mu N = 30\,\mathrm{N}$ in the simulations. The parameter ϵ defines the degree of regularization. A smaller ϵ gives a better estimate of the sign function, but convergence issues rise as the nonlinear force gets close to being effectively discontinuous. In order to account of the sticking state at low vibration levels, a relatively small value of ϵ is required. On the other hand, at high vibration level, the value retained for ϵ at low amplitude would make the convergence of the solver extremely hard, with yet no significant changes in the solution. This parameter is thus chosen so as to ensure a good compromise between computational cost and accuracy, varying in the numerical simulations from 4×10^5 at low amplitude to 2×10^3 at high amplitude.

The wave approach developed in Section 4 is used here to simulate the steady-state nonlinear behavior of the beam. The transmission/reflection coefficients at the discontinuity created by the friction force are given in Appendix C. Numerical values for the simulations are: total length of the beam: $L = 1.5\,\mathrm{m}$; position of the nonlinear force along the beam: $L/4$; beam cross section: 1 cm by 10 cm; material $\rho = 7850\,\mathrm{kg/m^3}$, $E = 200\,\mathrm{GPa}$, $\eta = 10^3$; $\epsilon = 7 \times 10^{-4}$; and $F_1 = 2\,\mathrm{N}$. The AFT-scheme used (see section 4.3) was performed with 512 time-discrete samples to ensure enough accuracy in the evaluation of the nonlinear force over one period of vibration.

We first study the influence of the harmonics number on the amplitude of motion and compare the results with direct time integrations performed on an FE model discretized with 20 elements. This is illustrated in Fig. 10. The frequency response shown in Fig. 10a shows that the tip displacement converges, for a sufficiently large number of harmonics N_h, towards direct time integration results. The number of harmonics needed for convergence is relatively high (here = 31) mainly because linear

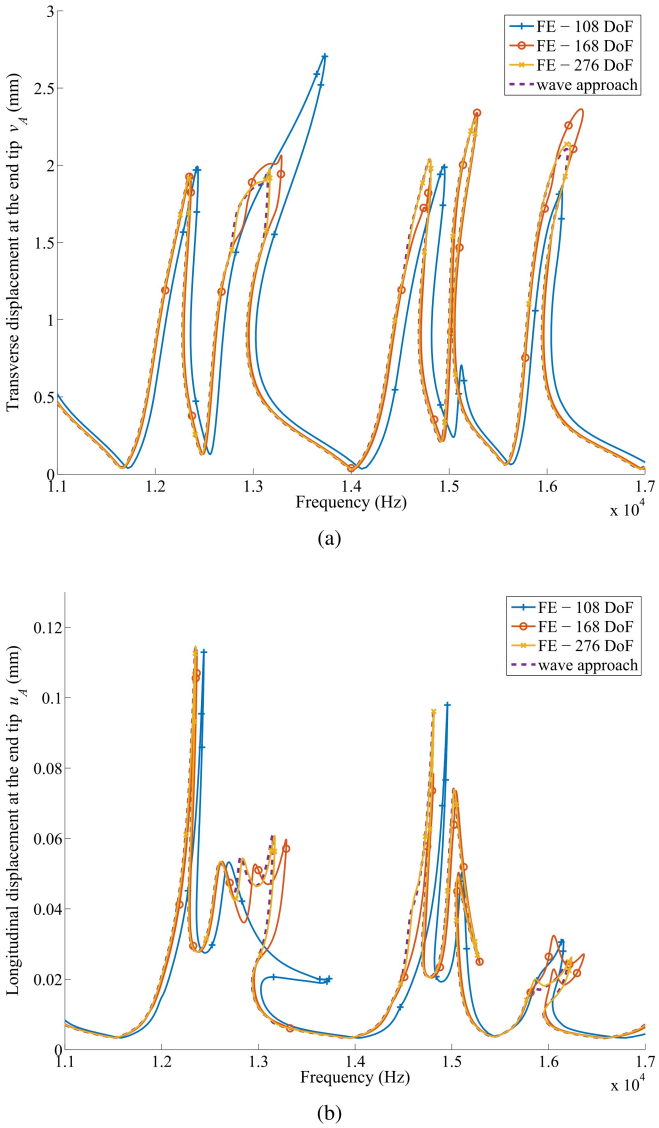

Fig. 8. Nonlinear response in A at high frequency; comparison between the wave approach and FE simulations with different number of degrees of freedom (DoF). (a) – transverse displacement (v), and (b) – longitudinal displacement (u).

damping was set very small and nonlinear effects dominate. The key feature defining the quality of the solution is the accuracy with which the motion of the friction point can be approximated. A sufficient number of harmonics must be kept to account for the stick-slip transitions occurring at the contact point when the nonlinearity is activated. To illustrate this, the transverse displacement of the contact point v_B is plotted in Fig. 10b for different values of N_h as a function of time over one period T. The excitation frequency is fixed and equal to 4.7 Hz.[3] The accuracy with which this temporal pattern is approximated directly affects the response in amplitude at the tip of the beam. The displacement computed by the wave approach converges toward time integration results but a large number of N_h is needed for a good approximation. However, it is actually not a numerically big effort[4] to compute the response with $N_h = 31$ because: (i) the number of unknowns is relatively low ($= 16N_h$ without the 'static terms' of Eq. (14)), (ii) an analytical expression of the Jacobian matrix of the system (12) was given to the solver, as suggested in Ref. [29].

On systems with such dampers, a frequency shift is classically observed when the amplitude of motion is increased [28,34] due to the softening effect arising from the friction. This is illustrated in Fig. 11. In this figure, the tip compliance (amplitude over

[3] This corresponds to the red circle in Fig. 10a.

[4] Runtime of less than 5 min with MATLAB R2014a and a 2.1 GHz Intel Core i7 laptop with 16Go RAM.

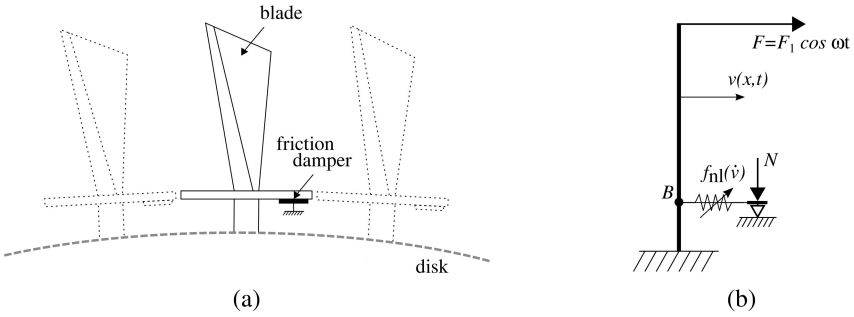

Fig. 9. Blade-to-ground underplatform damper: (a) schematic representation, (b) representative model.

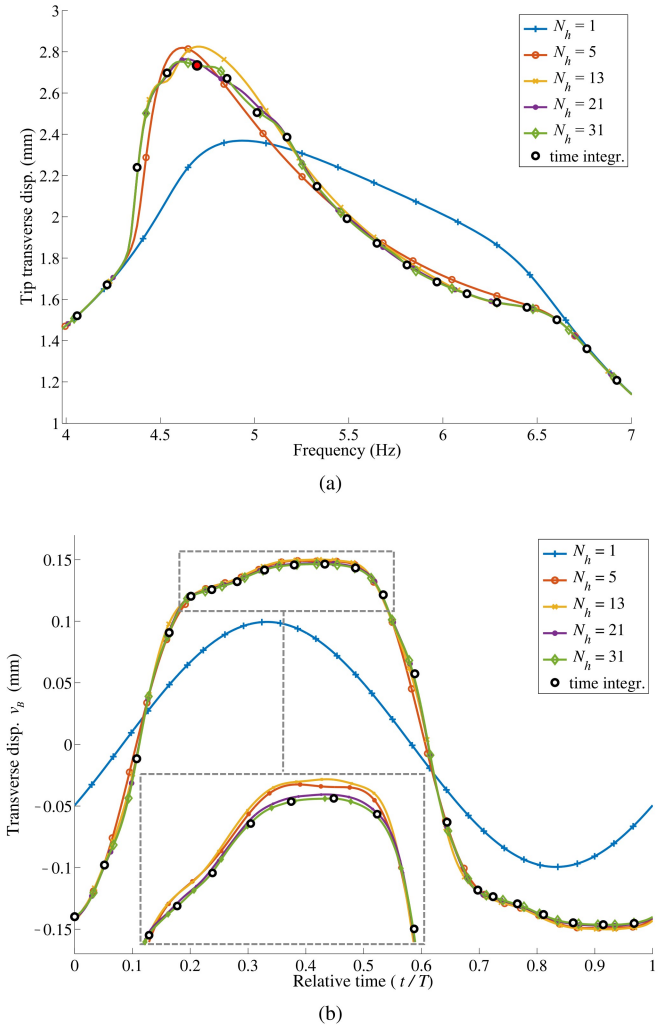

Fig. 10. Steady-state response of the beam with a dry friction damper for different N_h-values. Comparison with numerical time integration. (a) Tip displacement function of the excitation frequency, (b) Evolution of the contact point displacement over one period T.

force) is plotted as a function of the excitation frequency and for different levels of forcing. The resonant peak frequency varies indeed between the corresponding linear natural frequencies of the underlying system with bonded and frictionless interface, at low and high level of forcing F_1 respectively. These results also show an optimum value of damping for which the vibration mitigation is maximum. It occurs in our case for an excitation level F_1 of approximately 2 N. This behavior is rather standard and is generally demonstrated with lumped parameters models (in Refs. [28,29] for instance).

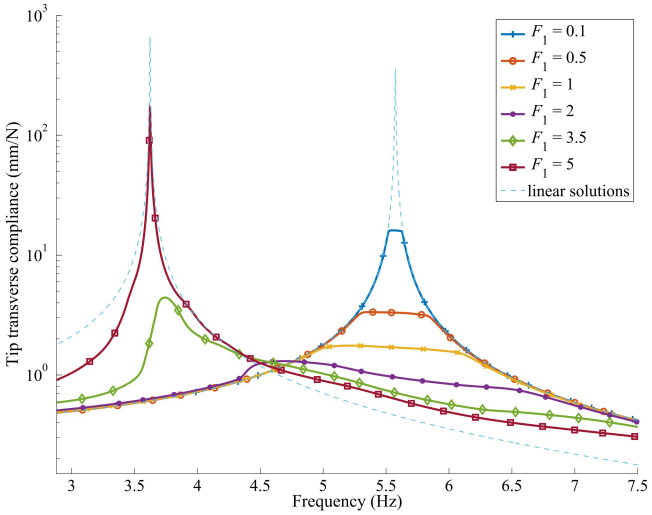

Fig. 11. General behavior of the compliance at the beam tip for different excitation level F_1 (in N) with respect to the bounded and frictionless linear responses.

Lumped parameter models have been widely used to study friction. Beside from being numerically cheap to compute for parametric studies, they can provide some interesting and valuable qualitative results. The size of the present wave approach model, in terms of number of variables, is equivalent to a 8 DoF lumped model. The approach we propose then offers the same benefits of low computational cost but with some valuable additional information as the model is continuous. This may be of particular interest for the study of power flow or vibration transmission between components. Furthermore high frequency response can also be computed accurately if required, which is not the case for a lumped element model.

6. Conclusions

This paper has proposed a method to simulate the free (nonlinear modes) and forced steady-state response of a beam-like network with localized nonlinearities. The overall procedure is motivated by the fact that beam-like structures are often used for optimization purpose in a pre-dimensioning design step and that the consideration of nonlinear effects makes detailed FE models cumbersome to use in practice.

This paper has extended an existing matrix-based wave approach methodology to deal with nonlinear vibrations in beam elements. The displacements are defined with waves traveling in the different elements at speeds associated with the fundamental excitation frequency and its multiples. Harmonic balance is then used to obtain an algebraic system of equations with wave amplitudes as unknowns. The proposed wave-based methodology offers several advantages compared to discretization method, among which (i) a better accuracy than Rayleigh-Ritz or modal approach as one solves for the exact continuous solution of the problem, and (ii) a significant decrease in the number of variables compared to a finely discretized FE model. Those benefits are common to the linear case but they are even more relevant for nonlinear analyses as the numerical cost to solve the nonlinear problem generally greatly increases. However, beside the fact that it may only model one-dimensional waveguide structures, the limitations of the proposed method are the same as those of a classical HB method. The main ones are the fact that: (i) one only looks for a periodic response (quasi-periodic, chaotic, and transient behavior cannot be captured) whose approximation is made by harmonic functions, and (ii) the nonlinear effect is also projected onto a Fourier basis, which may be an important approximation for non-continuous nonlinearities.

The methodology was first applied to simple academic structures. The calculation of transmission/reflection coefficients, the assembly procedure and the nonlinear force consideration in the wave approach were validated by comparison with an FE analysis supplemented by an HB method, and with results from direct time integration. It showed perfect agreement with an important numerical cost reduction. It was also applied to a more practical problem, namely a representative model of a turbine blade with underplatform damping. A parameter study was performed to show the influence of the external forcing amplitude on the nonlinear damping, and exhibits an optimum maximum damping for vibration mitigation. This example has also demonstrated that the number of harmonics retained in the periodic approximation is a key parameter in the model: it must be high enough to correctly predict the non-smooth stick-slip behavior occurring at the friction interface.

As further work to extend the current formulation, one could think of developing a methodology to analyse the stability of the different branches in the vibrational response and considering nonlinear vibrations in Timoshenko beams and/or out-of-plane vibration for modeling more general structures.

Acknowledgement

This research did not receive any specific grant from funding agencies in the public, commercial, or not-for-profit sectors.

Appendix A. Linear shape functions

This appendix gives details of the classical shape functions used in Eqs. (4) and (14) for longitudinal and transverse displacements of a beam element. The beam element (m) has a length L and the longitudinal displacement, transverse displacement, and slope of its left ($x = 0$) and right ($x = L$) nodes are respectively $U_1^{(\mathrm{m})}$, $V_1^{(\mathrm{m})}$ and $V_2^{(\mathrm{m})}$, and $U_2^{(\mathrm{m})}$, $V_3^{(\mathrm{m})}$ and $V_4^{(\mathrm{m})}$.

The static longitudinal and transverse displacements are defined by:

$$u(x) = \sum_{i=1}^{2} U_i^{(\mathrm{m})} N_i^l(x) \quad \text{and} \quad v(x) = \sum_{i=1}^{4} V_i^{(\mathrm{m})} N_i^f(x)$$

where the shape functions used are: $N_1^l(x) = 1 - \epsilon$, $N_2^l(x) = \epsilon$, $N_1^f(x) = 1 - 3\epsilon^2 + 2\epsilon^3$, $N_2^f(x) = L(\epsilon - 2\epsilon^2 + \epsilon^3)$, $N_3^f(x) = 3\epsilon^2 - 2\epsilon^3$, $N_4^f(x) = L(\epsilon^3 - \epsilon^2)$, with $\epsilon = x/L$.

Appendix B. Projection of the equations governing the discontinuities in the simple bar example

The equations governing the discontinuities in the example described in Section 3.2 are projected with the scalar product (5) to give the following equations, $\forall p \in [\![1, N_h]\!]$:

Left boundary

$$< (6), 1 > \quad EA\left(\frac{U_2^{(1)} - U_1^{(1)}}{L}\right) = k_1 U_1^{(1)} + \frac{1}{2} < f_{\mathrm{nl}}^{[1]}, 1 > \tag{B.1}$$

$$< (6),\, e^{\mathrm{i}p\omega t} > \quad \mathrm{i}EApk_l\left(-\hat{u}_p^{(1)+} + \hat{u}_p^{(1)-} e^{-\mathrm{i}pk_l L}\right) = (k_1 + \mathrm{i}cp\omega)\left(\hat{u}_p^{(1)+} + \hat{u}_p^{(1)-} e^{-\mathrm{i}pk_l L}\right) + < f_{\mathrm{nl}}^{[1]},\, e^{\mathrm{i}p\omega t} > \tag{B.2}$$

Right boundary

$$< (7), 1 > \quad U_2^{(2)} - U_1^{(2)} = 0 \tag{B.3a}$$

$$< (7),\, e^{\mathrm{i}p\omega t} > \quad -\hat{u}_p^{(2)+} e^{-\mathrm{i}pk_l l} + \hat{u}_p^{(2)-} = 0 \tag{B.3b}$$

Point force

Displacement continuity at application point:

$$< (8\mathrm{a}), 1 > \quad U_2^{(1)} = U_1^{(2)} \tag{B.4a}$$

$$< (8\mathrm{a}), e^{\mathrm{i}p\omega t} > \quad \hat{u}_p^{(1)+} e^{-\mathrm{i}pk_l L} + \hat{u}_p^{(1)-} = \hat{u}_p^{(2)+} + \hat{u}_p^{(2)-} e^{-\mathrm{i}pk_l l}. \tag{B.4b}$$

Force equilibrium at application point:

$$< (8\mathrm{b}), 1 > \quad F_0 = EA\left(\frac{U_2^{(1)} - U_1^{(1)}}{L} - \frac{U_2^{(2)} - U_1^{(2)}}{l}\right) \tag{B.5a}$$

$$< (8\mathrm{b}), e^{\mathrm{i}p\omega t} > \quad F_p = \mathrm{i}EApk_l\left(-\hat{u}_p^{(1)+} e^{-\mathrm{i}pk_l L} + \hat{u}_p^{(1)-} + \hat{u}_p^{(2)+} - \hat{u}_p^{(2)-} e^{-\mathrm{i}pk_l l}\right). \tag{B.5b}$$

Appendix C. Transmission and reflection coefficients

The linear transmission/reflection coefficients at common boundaries (such as clamped or free) and at the right angle of Fig. 4 can be found in Ref. [12].

At the right boundary of Fig. 4, the discontinuity is characterized by a viscous damper, a linear stiffness and a nonlinear stiffness. The associated reflection coefficients that link incoming waves (positive x-direction traveling waves, superscript $^+$), which have traveled along a length L before the discontinuity, to created or reflected waves (negative x-direction traveling waves, superscript $^-$) are defined with the following relations, $\forall p \in [\![1, N_h]\!]$:

$$\hat{u}_p^- = e^{-\mathrm{i}pk_l L}\hat{u}_p^+, \tag{C.1}$$

$$\begin{bmatrix}\hat{v}_p^- \\ \hat{w}_p^-\end{bmatrix} = \frac{1}{\gamma}\begin{bmatrix}-(\mathrm{i}+1)\alpha - 2\beta & 2\alpha \\ -2\mathrm{i}\alpha & (\mathrm{i}+1)\alpha - 2\beta\end{bmatrix}\begin{bmatrix}e^{-\mathrm{i}\sqrt{p}k_f L}\hat{v}_p^+ \\ e^{-\sqrt{p}k_f L}\hat{w}_p^+\end{bmatrix} + \frac{f_{\mathrm{nl},p}^{[A]}}{\gamma}\begin{bmatrix}1\\1\end{bmatrix}, \tag{C.2}$$

where:

$$\alpha = EIk_f^3 p^{3/2}, \qquad \beta = -k_1 - \mathrm{i}pc\omega, \qquad \gamma = (1-\mathrm{i})\alpha + 2\beta,$$

$$f_{\mathrm{nl},p}^{[A]} = < k_2 v_A^2 + k_3 v_A^3,\ e^{\mathrm{i}p\omega t} >$$

Concerning the beam with a dry friction damper (Fig. 9b), the discontinuity in B is characterized by the relation, $\forall p \in [\![1, N_h]\!]$:

$$\begin{bmatrix}\hat{v}_p^{(1)-} \\ \hat{w}_p^{(1)-} \\ \hat{v}_p^{(2)+} \\ \hat{w}_p^{(2)+}\end{bmatrix} = \begin{bmatrix}0&0&1&0\\0&0&0&1\\1&0&0&0\\0&1&0&0\end{bmatrix}\begin{bmatrix}e^{-\mathrm{i}\sqrt{p}k_f L^{(1)}}\hat{v}_p^{(1)+} \\ e^{-\sqrt{p}k_f L^{(1)}}\hat{w}_p^{(1)+} \\ e^{-\mathrm{i}\sqrt{p}k_f L^{(2)}}\hat{v}_p^{(2)-} \\ e^{-\sqrt{p}k_f L^{(2)}}\hat{w}_p^{(2)-}\end{bmatrix} + \frac{f_{\mathrm{nl},p}^{[B]}}{4\alpha}\begin{bmatrix}\mathrm{i}\\1\\\mathrm{i}\\1\end{bmatrix} \tag{C.3}$$

with:

$$f_{\mathrm{nl},p}^{[B]} = < \mu N \tanh\frac{\dot{v}_B}{\epsilon},\ e^{\mathrm{i}p\omega t} >,$$

where $\dot{v}_B$ is the transverse velocity of point B, and the beam elements on each side of the discontinuity are numbered (1) (length $L^{(1)}$) and (2) (length $L^{(2)}$). The linear transmission coefficients defining this discontinuity are actually equal to 1 because the discontinuity is purely nonlinear.

References

[1] M. Legrand, C. Pierre, P. Cartraud, J.P. Lombard, Two-dimensional modeling of an aircraft engine structural bladed disk-casing modal interaction, J. Sound Vib. 319 (2009) 366–391, https://doi.org/10.1016/j.jsv.2008.06.019.

[2] P. Almeida, C. Gibert, F. Thouverez, X. Leblanc, J.-P. Ousty, Numerical analysis of bladed disk–casing contact with friction and wear, J. Eng. Gas Turbines Power 138 (2016) 122802, https://doi.org/10.1115/1.4033065.

[3] L. Pešek, M. Hajžman, L. Půst, V. Zeman, M. Byrtus, J. Brůha, Experimental and numerical investigation of friction element dissipative effects in blade shrouding, Nonlinear Dynam. 79 (3) (2015) 1711–1726, https://doi.org/10.1007/s11071-014-1769-3.

[4] K.-Y. Jhang, Nonlinear ultrasonic techniques for nondestructive assessment of micro damage in material: a review, Int. J. Precis. Eng. Manuf. 10 (1) (2009) 123–135, https://doi.org/10.1007/s12541-009-0019-y.

[5] S.C. Stanton, C.C. McGehee, B.P. Mann, Nonlinear dynamics for broadband energy harvesting: investigation of a bistable piezoelectric inertial generator, Phys. D Nonlinear Phenom. 239 (10) (2010) 640–653, https://doi.org/10.1016/j.physd.2010.01.019.

[6] X.-F. He, J. Gao, Wind energy harvesting based on flow-induced-vibration and impact, Microelectron. Eng. 111 (2013) 82–86, https://doi.org/10.1016/j.mee.2013.02.009.

[7] M. Rezaei, S.E. Khadem, P. Firoozy, Broadband and tunable pzt energy harvesting utilizing local nonlinearity and tip mass effects, Int. J. Eng. Sci. 118 (2017) 1–15, https://doi.org/10.1016/j.ijengsci.2017.04.001.

[8] H. Jalali, H. Ahmadian, F. Pourahmadian, Identification of micro-vibro-impacts at boundary condition of a nonlinear beam, Mech. Syst. Signal Process. 25 (3) (2011) 1073–1085, https://doi.org/10.1016/j.ymssp.2010.09.007.

[9] F. Georgiades, A.F. Vakakis, Dynamics of a linear beam with an attached local nonlinear energy sink, Commun. Nonlinear Sci. Numer. Simulat. 12 (2007) 643–651, https://doi.org/10.1016/j.cnsns.2005.07.003.

[10] T.H. Richards, Y.T. Leung, An accurate method in structural vibration analysis, J. Sound Vib. 55 (3) (1977) 363–376, https://doi.org/10.1016/S0022-460X(77)80019-9.

[11] Y.H. Pao, W.Q. Chen, S. X. Y, The reverberation-ray matrix and transfer matrix analyses of unidirectional wave motion, Wave Motion 44 (6) (2007) 419–438, https://doi.org/10.1016/j.wavemoti.2007.02.004.

[12] B. Chouvion, C.H.J. Fox, S. McWilliam, A.A. Popov, In-plane free vibration analysis of combined ring-beam structural systems by wave propagation, J. Sound Vib. 329 (2010) 5087–5104, https://doi.org/10.1016/j.jsv.2010.05.023.

[13] L. Tang, D. Huang, R. Cao, H. He, Vibration analysis of a multi-span rotating ring with ray tracing method, Wave Motion 52 (2015) 91–102, https://doi.org/10.1016/j.wavemoti.2014.09.003.

[14] B.R. Mace, Wave reflection and transmission in beams, J. Sound Vib. 97 (1984) 237–246, https://doi.org/10.1016/0022-460X(84)90320-1.

[15] B.R. Mace, Power flow between two continuous one-dimensional subsystems: a wave solution, J. Sound Vib. 154 (2) (1992) 289–319, https://doi.org/10.1016/0022-460X(92)90583-J.

[16] C. Mei, B.R. Mace, Wave reflection and transmission in timoshenko beams and wave analysis of timoshenko beam structures, J. Vib. Acoust. 127 (4) (2004) 382–394, https://doi.org/10.1115/1.1924647.

[17] X.Q. Wang, R.M.C. So, Various standing wave in a timoshenko beam, J. Sound Vib. 280 (2005) 311–328, https://doi.org/10.1016/j.jsv.2003.12.012.
[18] K.T. Chan, X.Q. Wang, R.M.C. So, J. Huang, Revolving superposed standing waves in a spinning timoshenko beam, J. Sound Vib. 331 (2012) 815–832, https://doi.org/10.1016/j.jsv.2011.09.013.
[19] K.F. Graff, Wave Motion in Elastic Solids, Ohio State University Press, 1975.
[20] L. Cremer, M. Heckl, E.E. Ungar, Structure-borne Sound, Springer-Verlag, Munich, 1988.
[21] D. Duhamel, B.R. Mace, M.J. Brennan, Finite element analysis of the vibrations of waveguides and periodic structures, J. Sound Vib. 294 (1–2) (2006) 205–220, https://doi.org/10.1016/j.jsv.2005.11.014.
[22] J.M. Renno, B.R. Mace, Calculation of reflection and transmission coefficients of joints using a hybrid finite element/wave and finite element approach, J. Sound Vib. 332 (2013) 2149–2164, https://doi.org/10.1016/j.jsv.2012.04.029.
[23] A.F. Vakakis, Scattering of structural waves by nonlinear elastic joints, J. Vib. Acoust. 115 (4) (1993) 403–410, https://doi.org/10.1115/1.2930364.
[24] M.J. Brennan, E. Manconi, B. Tang, V. Lopes Jr., Wave reflection at the end of a waveguide supported by a nonlinear spring, in: Eurodyn 2014: IX International Conference on Structural Dynamics. Munich, 2014.
[25] B. Chouvion, A.A. Popov, S. McWilliam, C.H.J. Fox, Vibration modelling of complex waveguide structures, Comput. Struct. 89 (2011) 1253–1263, https://doi.org/10.1016/j.compstruc.2010.08.010.
[26] T.M. Cameron, J.H. Griffin, An alternating frequency/time domain method for calculating the steady-state response of nonlinear dynamic systems, J. Appl. Mech. 56 (1) (1989) 149–154, https://doi.org/10.1115/1.3176036.
[27] D. Charleux, C. Gibert, F. Thouverez, J. Dupeux, Numerical and experimental study of friction damping blade attachments of rotating bladed disks, Int. J. Rotating Mach. (2006) 1–13, https://doi.org/10.1155/IJRM/2006/71302.
[28] D. Laxalde, F. Thouverez, J.-J. Sinou, J.-P. Lombard, Qualitative analysis of forced response of blisks with friction ring dampers, Eur. J. Mech. A/Solid. 26 (4) (2007) 676–687, https://doi.org/10.1016/j.euromechsol.2006.10.002.
[29] C. Joannin, B. Chouvion, F. Thouverez, J.-P. Ousty, M. Mbaye, A nonlinear component mode synthesis method for the computation of steady-state vibration in non-conservative systems, Mech. Syst. Signal Process. 83 (2017) 75–92, https://doi.org/10.1016/j.ymssp.2016.05.044.
[30] A.H. Nayfeh, B. Balachandran, Applied Nonlinear Dynamics, Wiley-VCH Verlag GmbH, 1995, https://doi.org/10.1002/9783527617548.ch6.
[31] A.H. Nayfeh, D.T. Mook, Nonlinear Oscillations, Wiley-VCH Verlag GmbH, 2007, https://doi.org/10.1002/9783527617586.
[32] E.P. Petrov, D.J. Ewins, Effects of damping and varying contact area at blade-disk joints in forced response analysis of bladed disk assemblies, J. Turbomach. 128 (2) (2005) 403–410, https://doi.org/10.1115/1.2181998.
[33] S. Zucca, D. Di Maio, D.J. Ewins, Measuring the performance of underplatform dampers for turbine blades by rotating laser Doppler vibrometer, Mech. Syst. Signal Process. 32 (2012) 269–281, https://doi.org/10.1016/j.ymssp.2012.05.011.
[34] C. Gastaldi, A. Fantetti, T.M. Berruti, Forced response prediction of turbine blades with flexible dampers: the impact of engineering modelling choices, Appl. Sci. 8 (34) (2018) 1–20, https://doi.org/10.3390/app8010034.